SUPPLEMENTARY MATERIAL

PAALD process was employed to fabricate TiO_x films with various doping profiles. All procedures utilized 600 deposition cycles to ensure consistent film thickness. The process parameters are given Table S1.

Supplementary Table S1. Process procedures for PAALD films.

Procedure	O_2 (sccm)	H_2 (sccm)	N_2 (sccm)	Plasma time (H_2) (s)	Plasma time (N_2) (s)	Number of Cycles
1	0	50	0	1	0	600
2	0	50	0	3	0	600
3	0	50	0	6	0	600
N-TiO_x	0	0	50	0	3	600
TiO_2	60	0	0	0	0	600

The raw and modeled data from the ellipsometer for each film are shown in Figure S1.

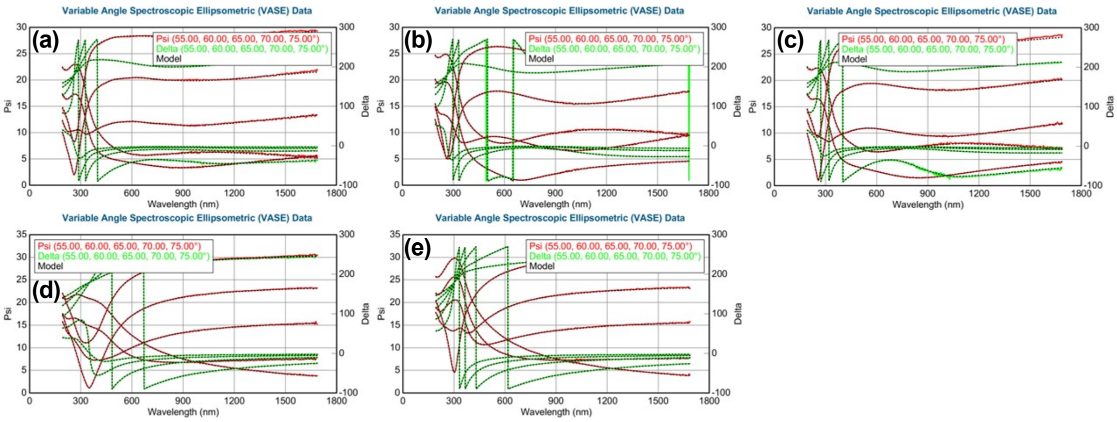

Supplementary Figure S1. Raw ellipsometer data and modeled B-spline fit for (a) H-TiO_x-1s, (b) H-TiO_x-3s, (c), H-TiO_x-6s, (d) N-TiO_x, and TiO_2 films.

From the physical model constructed by the ellipsometry measurements, the optical constants and absorption coefficients were determined as plotted in Figure S2.

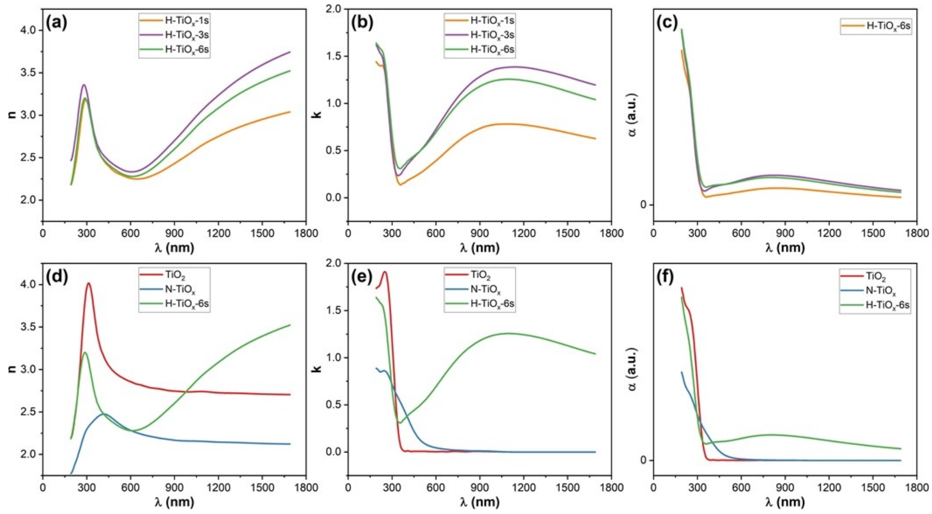

Supplementary Figure S2. Optical coefficients and absorption spectra of various TiO_x films.

For calculating the bandgap energies of the films, the Tauc plots were constructed using the absorption coefficients, α, extracted from the optical model of the ellipsometry. The energy-dependent absorption coefficient expressed with the following formula:

$$(\alpha h\nu)^{1/\gamma} = B(h\nu - E_g) \quad (3)$$

where h is the plank constant, ν is the frequency of the photon, B is a constant, and E_g is the bandgap energy. The factor γ depends on the nature of the electron transition and TiO_2 shows the indirect transition bandgap properties, therefore $\gamma = 2$ was used for all calculations. The energy-dependent absorption coefficient was plotted with respect to the photon energy $h\nu$ and E_g as shown in Figure 2a-b and the bandgap energies were determined by extrapolating the intersection of the horizontal axis and the curve from linear region [50].

The XPS survey spectra (Figure S3a) clearly show that the surfaces of ALD-grown TiO_x films are clean, with only a trace amount of C coming from air exposure. Ti, O, and C elements were found from the survey scan of TiO_2 and H-TiO_x films. Additionally, the N 1s peak was observed in N-TiO_x. Figure S3b shows the O1s spectra for the TiO_x films. The center peak that appeared at 530 eV is expected for O^{2-} anions of the TiO_2 structure, i.e. from the $Ti^{4+}-O^{2-}$ bond, while the peak at 531.6 eV is attributed to hydroxyl groups on the surface of the films. With introducing the N_2 plasma to lead the formation of N-TiO_x, the Ti−O bond intensity decreased, and adsorbed oxygen intensity increased. This is possibly because of the fact that the incorporation of nitrogen atoms into the films limits the Ti−O bond formation. Additionally, the peaks were shifted from 530 and 531.6 eV to 528.4 and 530 eV, respectively with N_2 plasma exposure. These shifts are because of the formation of Ti−N and Ti−O−N bonds as shown in XPS N 1s spectrum of N-TiO_x (Figure S3c). By H_2 plasma introduction, slight peak shifts were observed to lower binding energies with a new peak corresponding to Ti−OH bond formation.

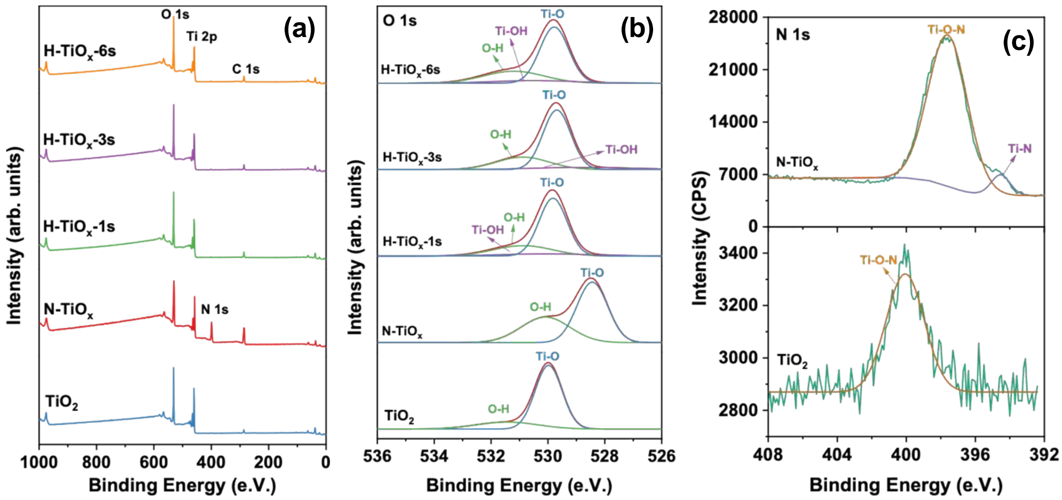

Supplementary Figure S3. XPS spectra of TiO_x films: (a) survey, (b) O 1s XPS spectra, and (c) N 1s XPS spectra of TiO_2 and N-TiO_x.

For the diode performance figure of merit, the responsivity is calculated using the following formula from measured IV-curves:

(4

$$\text{Responsivity} = \left(\frac{d^2I}{dV^2}\right) \Big/ \left(\frac{dI}{2dV}\right) \quad (4)$$

where I and V are the diode current and voltage, respectively. The numerator represents the second derivative of the current with respect to voltage, while the denominator is the product of the first derivative of the current with respect to voltage and twice the change in voltage.

Using equations 1 and 2, the relationship between the cutoff frequency, f_c, and diode resistance, R, is plotted in Figure S4.

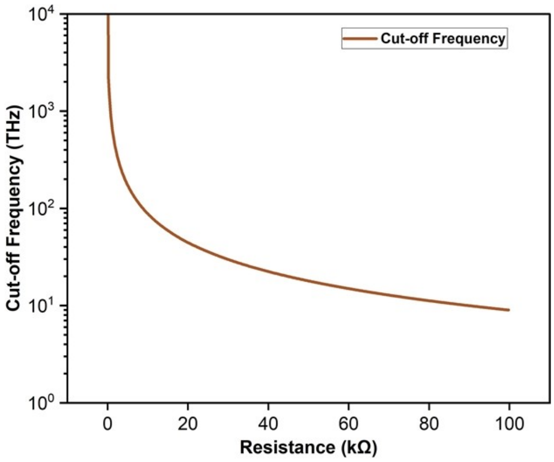

Supplementary Figure S4. The modeled cutoff frequency plot with respect to diode resistance.